



Investigation of the influence of asymmetrical profiles on the wear behavior in gear hobbing

C. Janßen¹ · J. Brimmers¹ · T. Bergs^{1,2}

Received: 30 November 2021 / Accepted: 18 December 2022 / Published online: 10 January 2023
© The Author(s) 2023

Abstract

Asymmetrical gears have advantages in applications with a preferred load direction, such as automotive transmissions or wind turbines. The operational behavior of gears with asymmetrical profiles has already been thoroughly investigated. However, there are very few studies on the manufacturability of gears with asymmetric profiles regarding the possible interactions between pressure angle composition, tool and process design. In this report, the influence of asymmetrical profiles on the wear behavior of hobs is analyzed for the first time.

For this purpose, eight different tool variants have been defined for an investigation on tool wear behavior based upon fly-cutting trials. These variants consist of two symmetric and four asymmetric variants. In addition, two asymmetric variants with additional protuberance have been defined. Tool performance decreased within the fly-cutting trials with a low pressure angle on the leading flank and also in the presence of a protuberance. As the pressure angle increases on the leading flank, an increase on the tool life was observed.

Untersuchung des Einflusses asymmetrischer Profile auf das Verschleißverhalten von Wälzfräsern

Zusammenfassung

Asymmetrische Zahnräder haben Vorteile bei Anwendungen mit einer Vorzugslastrichtung, wie z. B. bei Fahrzeuggetrieben oder Windkraftanlagen. Das Betriebsverhalten von Zahnrädern mit asymmetrischen Profilen ist bereits eingehend untersucht worden. Es gibt jedoch nur sehr wenige Studien über die Herstellbarkeit von Zahnrädern mit asymmetrischen Profilen im Hinblick auf die möglichen Wechselwirkungen zwischen Eingriffswinkelzusammensetzung, Werkzeug- und Prozessgestaltung. In diesem Bericht wird erstmals der Einfluss asymmetrischer Profile auf das Verschleißverhalten von Wälzfräsern analysiert.

Zu diesem Zweck wurden acht verschiedene Werkzeugvarianten für eine Untersuchung auf Basis von Schlagzahnversuchen definiert. Diese Varianten bestehen aus zwei symmetrischen und vier asymmetrischen Varianten. Darüber hinaus wurden zwei asymmetrische Varianten mit zusätzlicher Protuberanz definiert. Die Werkzeugstandlänge nahm bei den Schlagzahnversuchen mit einem geringen Eingriffswinkel an der einlaufenden Flankenseite und auch bei Vorhandensein einer Protuberanz ab. Mit zunehmendem Eingriffswinkel an der einlaufenden Flankenseite wurde eine Erhöhung der Standzeit beobachtet.

Availability of data and material not applicable

Code availability not applicable

✉ C. Janßen
c.janssen@wzl.rwth-aachen.de

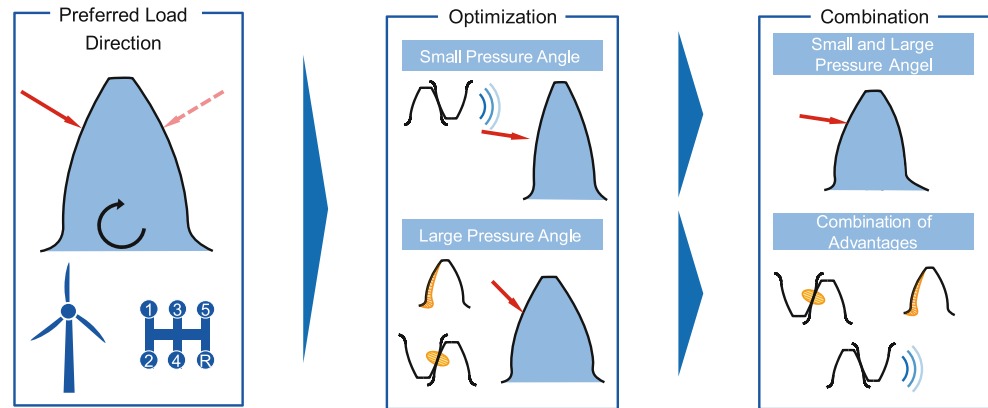
¹ WZL of RWTH Aachen University, Aachen, Germany

² Fraunhofer Institute for Production Technology IPT, Aachen, Germany

1 Introduction

The load carrying capacity of cylindrical gears is decisively influenced by the application-specific design of the gear macro geometry. Different pressure angles of the leading and trailing flanks can be used to achieve higher load carrying capacity and smoother running behavior compared to symmetrically designed gear profiles with the same pressure angles [1–3]. Asymmetrical spur gears are used today for special applications. However, the possible areas of use

Fig. 1 Advantages of gears with asymmetric profiles



could extend to all applications in which a load direction is preferred. Figure 1 shows two possible applications. Both automotive and wind turbine gearboxes have a preferred load direction. With a preferred load direction, it is possible to combine the advantages of small and large pressure angles that can result in gears with an improved excitation and load carrying behavior. In bevel gearboxes, e.g. differentials, the tooth geometry has been designed asymmetrically for years for the corresponding application [4–6].

Usually, gears for applications with high power density are pre-machined in soft state and then, after hardening, the desired surface quality is applied by grinding or honing [7]. During soft machining by gear hobbing, there are generally different loads on the tool flanks. It is not yet known to what extent asymmetrical designs of the pressure angles increase or decrease the predominant loads. This results in unknown effects on tool life and process stability, which makes it difficult to introduce asymmetrical gears despite their potential for increasing power density.

Gear hobbing has been investigated for several decades, particularly in e.g. [8–14]. The focus of these investigations is primarily on substrate- and coating-side productivity improvements, reprocessing, avoidance of surface defects in the dry hobbing process, and numerical tool life models for the hobbing process.

A comprehensive theoretical and experimental analysis of the influence of the gear geometry and the tool profile on the achievable tool life was carried out by Köchig. The investigations on different tool profiles showed clear dependencies between the respective tool profiles and the observed wear behavior [15].

At present, gear hobbing processes of asymmetric geometries are often designed iteratively because knowledge about the prevailing load conditions in the process is lacking. Furthermore, on the basis of the current state of knowledge, it is not possible to make any statement about possible interactions between pressure angle combination, tool and process design. However, the state of the art shows that gears with asymmetric profiles can significantly increase the

performance of gearboxes. Therefore, scientifically based knowledge is necessary to meet the manufacturing requirements of the gear hobbing process for asymmetrical gears in practice. The challenges in gear hobbing of asymmetrical gears lie in the special cutting conditions depending on the tool and process design.

The aim of this research is to investigate the tool life and wear behavior of hobs depending of asymmetrical profiles. For this purpose, tool profiles with different pressure angles are examined in the fly-cutting trial and the occurring tool wear is analyzed. For an initial theoretical consideration of the hobbing processes, a simulation regarding the maximum chip thickness $h_{cu,max}$ as an indication of the possible tool load is conducted.

2 Design of experiments

The experiments were carried out in an analogy trial for gear hobbing. For the analogy trial, the hob is replaced by a fly-cutter, which is separated from a solid hob. Consequently, the profile of the fly-cutter is the same as that of the original hob. During the cutting process, the fly-cutter is moved tangentially to the workpiece with a shift movement. The application of the shift motion allows the fly-cutter to reproduce any generating position of the hob

Table 1 Tool data

	Symbol	Value	Unit
Normal module	m_{n0}	2.557	mm
Pressure angle	α_{n0}	17.5	°
Addendum	h_{aP0}	4.31	mm
Tip radius	ρ_{aP0}	0.85	mm
Tip diameter	d_{a0}	80	mm
No. of gashes	n_{i0}	17	–
No. of starts	z_0	2, right	–
Substrate	–	S390	–
Coating	–	AICrN	–

Table 2 Gear data

	Symbol	Value	Unit
Normal module	m_{n2}	2.557	mm
Normal pressure angle	α_{n2}	17.5	°
Number of teeth	z_2	39	–
Helix angle	β_2	23	°
Gear width	b_2	30	mm
Tip diameter	d_{a2}	116.2	mm
Root diameter	d_{f2}	100.0	mm
Material	–	20MnCr5	–

for all gaps of the workpiece. The tool used was a right-handed hob with an outside diameter of $d_{a0} = 80$ mm, a number of gashes $n_{i0} = 17$, two starts z_0 and a normal module of $m_{n0} = 2.557$ mm. The investigated tool geometry corresponds to the WZL standard fly-cutter geometry [16]. The values are shown in Table 1.

The gear geometry investigated had a number of teeth of $z_2 = 39$, a normal module of $m_{n2} = 2.557$ mm, a helix angle of $\beta_2 = 23^\circ$ and a tip diameter of $d_{a2} = 116.2$ mm. The workpiece data is shown in Table 2. The tests were carried out on a Gleason Pfauter P400 gear hobbing machine. The manufacturing was carried out in climb cut without the use of cooling lubricant. The machine and the test setup for the fly-cutting trials are shown in Fig. 2.

The material used was 20MnCr5, a case-hardened steel with a ferritic-pearlitic matrix. An optical emission spectroscopy (OES) provided information on the chemical composition of the material which is represented in Table 3. The evaluation showed no deviations of the chemical composition from the standardized tolerance ranges [17]. A Brinell hardness of 170 HBW 2.5/62.5 was determined by hard-

Table 4 Coating chemical composition

wt%	Chrome	Aluminum	Nitrogen
AlCrN	43.6%	39.3%	17.2%

Table 5 Substrate chemical composition

wt%	Iron	Wolfram	Cobalt	Vanadium	Mangan
S390	70.7%	10.9%	7.7%	4.9%	0.8%

ness testing, which corresponds to a tensile strength of $R_m = 575$ MPa.

Based on the standard fly-cutting trial geometry, further variants were defined for the investigation of asymmetric profiles. For an isolated consideration of the influence of the asymmetric profiles on the wear behavior, the tip radius $\rho_{aP0} = 0.85$ mm was kept constant for all variants. To ensure a constant tip radius ρ_{aP0} , the sum of the pressure angles $\Sigma\alpha_{n,l/r} = 35^\circ$ was kept constant. The sum of the pressure angles $\Sigma\alpha_{n,l/r} = 35^\circ$ results from the symmetrical reference variant, which has a pressure angle of $\alpha_{n0} = 17.5^\circ$. In addition to the design of four asymmetric variants, two additional variants were defined which have a protuberance. An overview of all asymmetric variants and the design of experiments is given in Fig. 3.

The variants with pressure angles $\alpha_{n,l/r} = 12.5^\circ/22.5^\circ$ and $\alpha_{n,l/r} = 22.5^\circ/12.5^\circ$ were designed with a protuberance angle of $\alpha_{prP0,l/r} = 9^\circ/15^\circ$ and $\alpha_{prP0,l/r} = 15^\circ/9^\circ$, respectively. The protuberance height for both variants was $h_{prP0,l/r} = 2.309$ mm and $h_{prP0,l/r} = 1.076$ mm. In addition to the symmetric reference variant, another symmetric variant with a pressure angle of $\alpha_{n0} = 20^\circ$ was investigated. The fly-cutters used were taken from several hobs, which were manufactured from powder metallurgy high-speed steel (PM-HSS) S390. In addition, the hobs were coated with an AlCrN coating. The

Fig. 2 Experimental setup

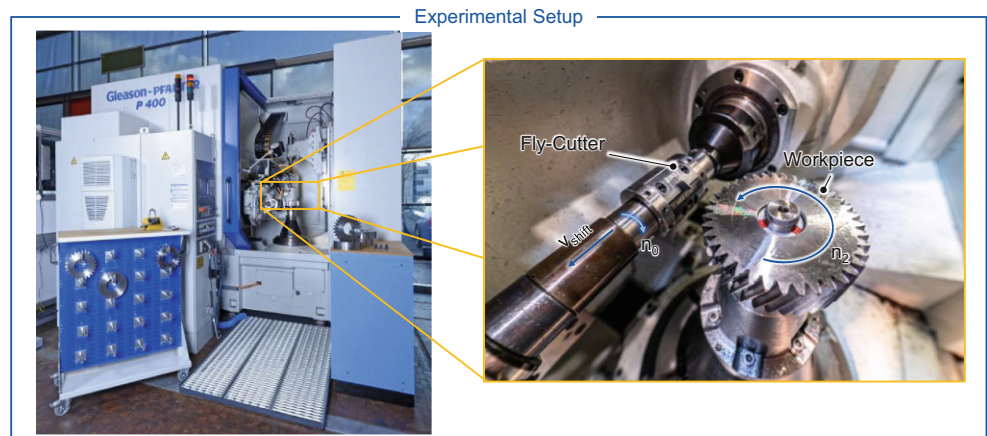


Table 3 Chemical composition of the investigated workpiece materials

wt%	C	Si	Mn	P	S	Cr	Mo	Ni	Al	Co	Cu
20MnCr5	0.20	0.24	1.14	0.016	0.022	1.06	1.060	0.026	0.024	0.010	0.02

Gear
 Material: 20MnCr5
 $z_2 = 39$
 $\beta_2 = 23^\circ$
 $d_{a2} = 116.2 \text{ mm}$

Tool
 Substrate: S390
 Coating: AlCrN
 $m_{n0} = 2.557 \text{ mm}$
 $\alpha_{n,l/r} = \text{variable}$
 $\rho_{aP0} = 0.85 \text{ mm}$
 $z_0 / n_{i0} = 17 / 2$
 $d_{a0} = 80 \text{ mm}$

Process
 Climb cut, dry
 $T = 8.1 \text{ mm}$
 $v_c = 200 \text{ m/min}$
 $f_a = 2.5 \text{ mm}$

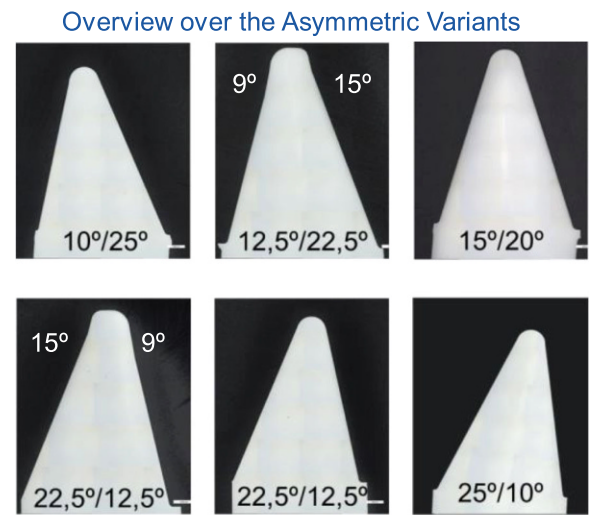
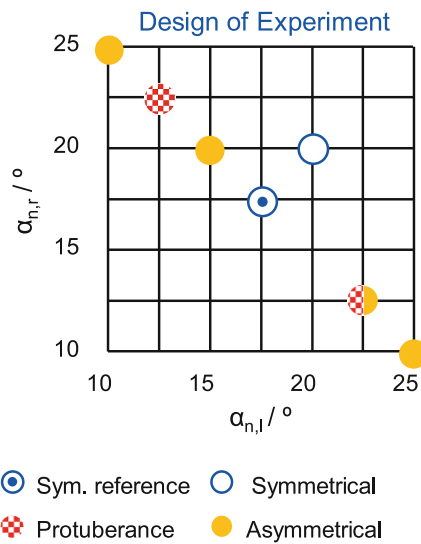


Fig. 3 Design of experiments and overview over asymmetric variants

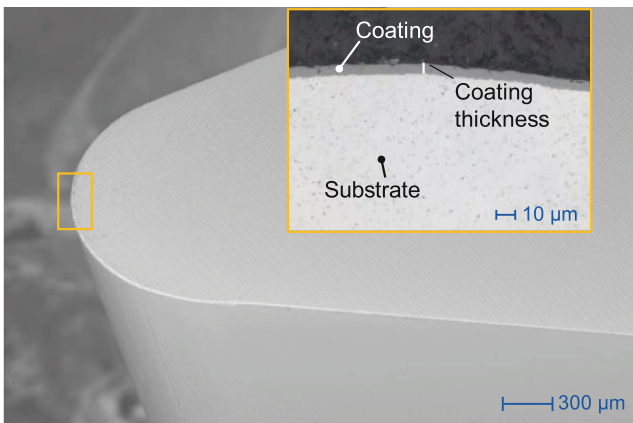


Fig. 4 Characterization of tool substrate and coating

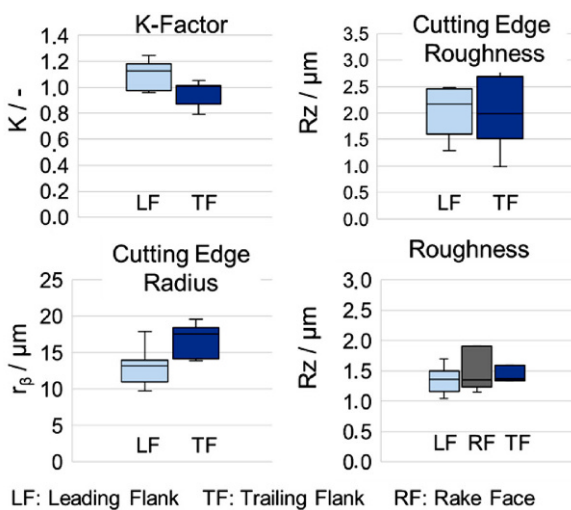


Fig. 5 Cutting edge preparation of all fly-cutters

characterization of the cutting material as well as the initial state of the fly-cutters is shown as an example in Fig. 4. Chemical analysis of the coating and the tool substrate was performed using energy dispersive X-ray microscopy (EDX) and are displayed in Table 4 and 5.

In addition to the optical analysis of the initial condition, further characteristic values such as the K-Factor, the roughness R_z of the cutting edge, the cutting edge rounding r_b and the roughness R_z of the rake and flank surfaces for all fly-cutters were determined. The results of the measurements are presented in the form of box-plot diagrams in Fig. 5. The average of the K-factor was $K \approx 1.1$ for the leading flank and $K \approx 0.95$ for the trailing flank. For the cutting edge roughness there were minor differences for both flank sides and was $R_z \approx 2 \mu\text{m}$. The measurement of the cutting edge radius r_b showed differences for the leading and trailing flanks. For the leading side, an average value of $r_b \approx 13 \mu\text{m}$ was measured. On the trailing flank, a slightly higher value of $r_b \approx 16 \mu\text{m}$ was measured. The roughness depth of the rake face was measured to be $R_z \approx 1.9 \mu\text{m}$ on average, which was higher than the values of the leading and trailing flanks with $R_z \approx 1.3 \mu\text{m}$ and $R_z \approx 1.4 \mu\text{m}$, respectively. The coating thickness at the tool tip was $s \approx 4.5 \mu\text{m}$ in average. A decrease of the coating thickness in the direction of the tooth root is to be expected due to the line-of-sight characteristics [18, 19].

3 Theoretical analysis

The theoretical analysis of gear hobbing with asymmetrical profiles was carried out using the SPARTApro manufacturing simulation. Based on tool, workpiece and process data, process-specific characteristic values were determined by

Gear
 $z_2 = 39$
 $\beta_2 = 23^\circ$
 $d_{a2} = 116.2 \text{ mm}$

Tool
 $m_{n0} = 2.557 \text{ mm}$
 $\alpha_{n,l/r} = \text{variable}$
 $\rho_{aP0} = 0.85 \text{ mm}$
 $z_0 / n_{i0} = 17 / 2$
 $d_{a0} = 80 \text{ mm}$

Process
 Climb cut, dry
 $T = 8.1 \text{ mm}$
 $v_c = 200 \text{ m/min}$
 $f_a = 2.5 \text{ mm}$

LF = Leading Flank
 TF = Trailing Flank

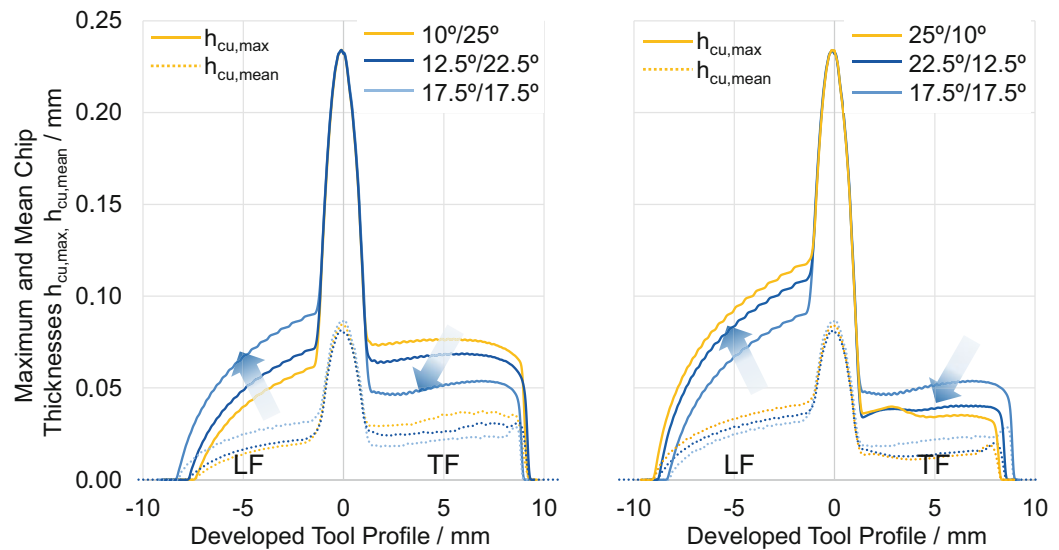


Fig. 6 Results of the calculation for the chip thickness $h_{cu,max}$ and $h_{cu,mean}$

means of geometric penetration calculation. Characteristic values, such as the mean chip thickness $h_{cu,mean}$ and maximum chip thickness $h_{cu,max}$, can be used as an indicator for stress on the tool cutting edge [20, 21]. Therefore these values can be used as an initial comparative values to investigate the influence of the pressure angle $\alpha_{n,l/r}$ on the development of the tool wear.

Figure 6 shows the diagrams of the maximum chip thickness $h_{cu,max}$ for the variants $\alpha_{n,l/r} = 10^\circ/25^\circ$, $\alpha_{n,l/r} = 12.5^\circ/22.5^\circ$ (in the left diagram) and $\alpha_{n,l/r} = 22.5^\circ/12.5^\circ$, $\alpha_{n,l/r} = 25^\circ/10^\circ$ (in the right diagram) as solid lines. In addition, the results of the symmetrical reference variant $\alpha_{n,l/r} = 17.5^\circ$ were compared for a classification of the progression of the chip thickness. The developed tool profile was divided into the areas of the leading flank (LF) and trailing flank (TF). An influence of varying pressure angles on the maximum chip thickness could not be identified. The maximum chip thickness occurs at the tool tip at $x_p = 0$. The geometry of the tool cutting edge at the tip is not influenced by a variation of the pressure angle, which is why a difference in the maximum chip thickness does not occur. In the area of the flanks however, an influence of the different pressure angles on the course of the maximum chip thickness $h_{cu,max}$ can be identified. By a decrease in the pressure angle on the trailing flank (from $\alpha_{n,r} = 25^\circ$ to $\alpha_{n,r} = 17.5^\circ$), the maximum chip thicknesses $h_{cu,max}$ decrease as well.

In contrast, the course of the maximum chip thickness $h_{cu,max}$ at the leading flank increases with increasing pressure angle. A similar trend can be observed for the variants $\alpha_{n,l/r} = 22.5^\circ/12.5^\circ$ and $\alpha_{n,l/r} = 25^\circ/10^\circ$. Reducing the pressure angle on the trailing flank also results in lower values of the maximum chip thickness $h_{cu,max}$ along the trailing. If, in return, the pressure angle on the leading flank increases, in-

creasing values of the maximum chip thickness $h_{cu,max}$ can be identified. From this it can be deduced that the mechanical load on the leading flank decreases with decreasing pressure angle and the mechanical load on the trailing flank increases accordingly. An equivalent behavior for the course of the chip thickness can be observed for the mean chip thickness $h_{cu,mean}$. In the area of the tool tip at $x_p = 0$, the mean chip thickness $h_{cu,mean}$ is constant for all variants shown. In the area of the leading and trailing flank, there is a change in the magnitude of the mean chip thickness $h_{cu,mean}$ due to the changing pressure angle. With increasing pressure angle, the amount of the mean chip thickness $h_{cu,mean}$ increases. With a reduction of the pressure angle, there is a decrease in the amount of the mean chip thickness $h_{cu,mean}$, analogous to the maximum chip thickness $h_{cu,max}$. Since the amount of the chip thicknesses ($h_{cu,max} = 0.05 \text{ mm}$ and $h_{cu,mean} = 0.03 \text{ mm}$) in the area of the leading flank do not fall below the radius of the cutting edge ($r_p \leq 0.017 \mu\text{m}$). Thus, an undercutting of the minimum chip thickness as a reason for higher wear can be ruled out on the clearance surface (see Fig. 5 and 6; [22]).

4 Fly-cutting trials

A maximum permissible wear mark width of $VB_{max,perm} = 250 \mu\text{m}$ and a maximum permissible crater depth of $KT_{max,perm} = 150 \mu\text{m}$ were defined as wear criteria. In addition, the tests were carried out until an exponential wear rate was achieved. The wear was measured at five positions on the clearance flanks after each machined workpiece. Measurements were taken at the tip and at the leading and trailing flank. The leading and trailing flank were addi-

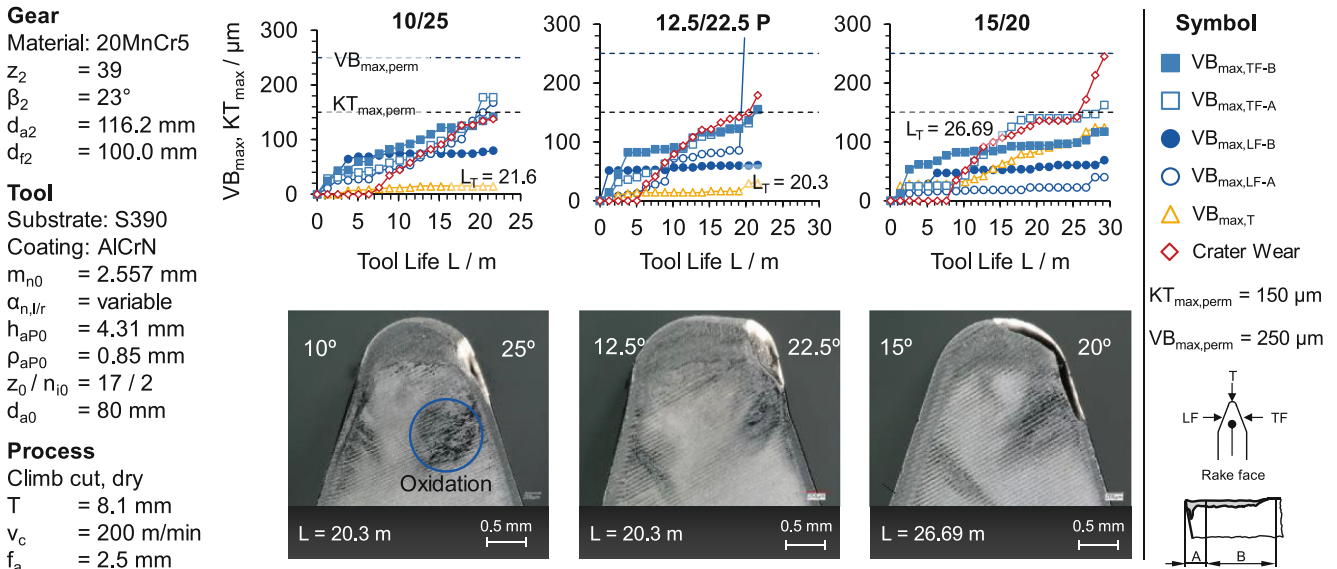


Fig. 7 Results for the fly-cutting trials for the variants 10/25, 12.5/22.5 P and 15/20

tionally divided into areas A and B. Area A includes the tip rounding of the tool, while area B includes the lower area of the tool flank. Furthermore, the crater wear on the rake face was documented. If the wear criterion was not reached, a further workpiece was machined. This process was repeated until either the permissible wear mark width or the permissible crater depth was reached. Accordingly, a test point in Fig. 7 corresponds to a machined workpiece.

For a better comparability, the number of machined workpieces N is converted into the machined length L according to Eq. 1. The tool life L_T describes the machined length at which the wear criterion is reached. The width, helix angle and the number of teeth of the workpiece are represented as b_2 , β_2 and z_2 .

$$L = \frac{N \cdot b_2 \cdot z_2}{\cos(\beta_2)} \tag{1}$$

Figure 7 shows the results of the fly-cutting trials of the variants with a pressure angle $\alpha_{n,l/r} = 10^\circ/25^\circ$, $\alpha_{n,l/r} = 12.5^\circ/22.5^\circ$ P (including protuberance) and $\alpha_{n,l/r} = 15^\circ/20^\circ$. With the exception of the $\alpha_{n,l/r} = 10^\circ/25^\circ$ variant, the exponential wear range was achieved for the regarded variants. In the variant $\alpha_{n,l/r} = 10^\circ/25^\circ$, the fly-cutter broke prematurely. All three variants shown have in common that the wear developed on the trailing flank. In addition, a progressive development of the crater wear can be identified.

For the variants with pressure angles $\alpha_{n,l/r} = 10^\circ/25^\circ$ and $\alpha_{n,l/r} = 12.5^\circ/22.5^\circ$, wear on the leading flank developed in addition to the flank wear on the trailing flank. Particularly for the variant $\alpha_{n,l/r} = 12.5^\circ/22.5^\circ$, the wear on the leading flank increased exponentially, as a result of which the maximum permissible wear mark width of $VB_{max,perm} = 250 \mu\text{m}$ was reached and the test was terminated.

Furthermore, a discoloration (highlighted in a blue circle) could be identified on the rake face of the variant $\alpha_{n,l/r} = 10^\circ/25^\circ$. This discoloration may indicate oxidation of the corresponding areas on the rake face, which, if more pronounced, may indicate chip flow obstructions [23]. While the two variants $\alpha_{n,l/r} = 10^\circ/25^\circ$ and $\alpha_{n,l/r} = 12.5^\circ/22.5^\circ$ with a tool life of $L_T = 21.6 \text{ m}$ and $L_T = 20.3 \text{ m}$ have an almost identical tool life, the variant $\alpha_{n,l/r} = 15^\circ/20^\circ$ with $L_T = 26.69 \text{ m}$ achieved a significantly higher tool life.

An overview of the results of the fly-cutter tests for the symmetrical variants with pressure angles $\alpha_n = 17.5^\circ$ and $\alpha_n = 20^\circ$ is given in Fig. 8. Analogous to the previously observed wear development, the wear is mainly formed on the trailing flank.

In addition, crater wear occurred on the rake face of both variants. The development of the crater wear was almost identical to the wear on the trailing flank in area A. When the exponential wear rate at the trailing flank was reached, the maximum wear criterion $VB_{max,perm} = 250 \mu\text{m}$ of the variant with a pressure angle $\alpha_n = 20^\circ$ was also exceeded. With a value of $L_T = 24.15 \text{ m}$, a higher tool life was achieved than for the symmetrical reference variant with a tool life of $L_T = 19.1 \text{ m}$.

Figure 9 shows the results of the fly-cutting trials of the variants with pressure angles $\alpha_{n,l/r} = 22.5^\circ/12.5^\circ$, $\alpha_{n,l/r} = 22.5^\circ/12.5^\circ$ P and $\alpha_{n,l/r} = 25^\circ/10^\circ$. For all three variants shown, the wear occurred mainly on the trailing flank. In addition, a progressive development of crater wear was observed. In contrast to the variants with mirrored pressure angles ($\alpha_{n,l/r} = 10^\circ/25^\circ$ and $\alpha_{n,l/r} = 12.5^\circ/22.5^\circ$), an increased occurrence of flank wear on the leading flank was not observed. In addition, the exponential wear rate was achieved for all three variants. In the case of the variant

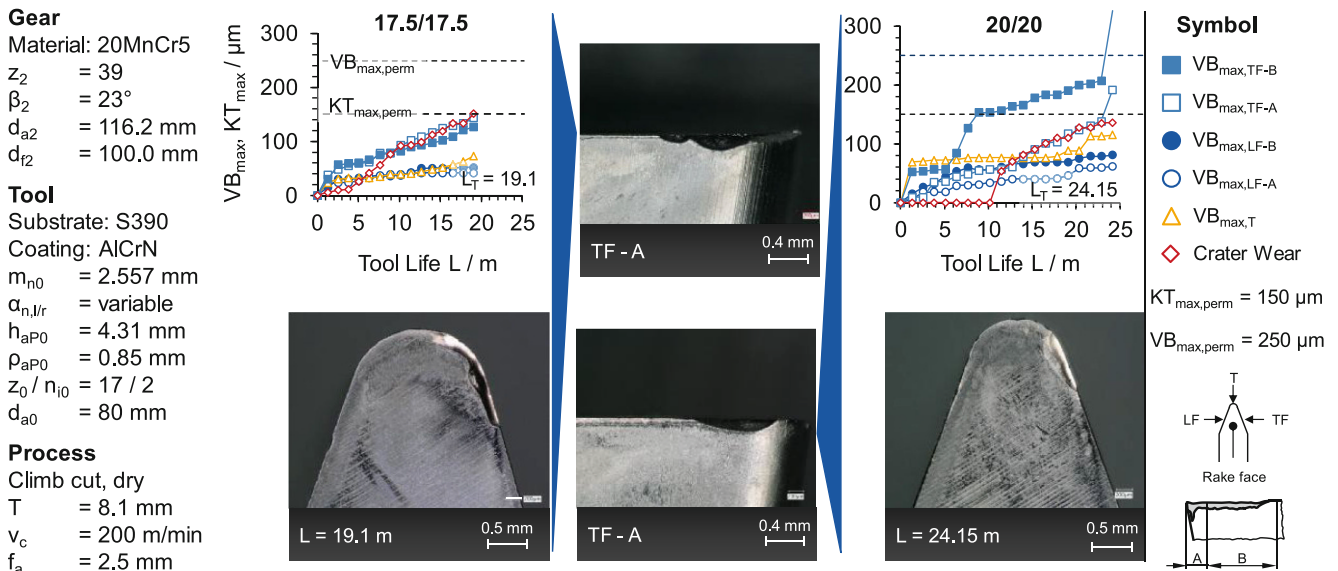


Fig. 8 Results for the fly-cutting trials for the symmetrical variants

with a pressure angle $\alpha_{n,l/r} = 25^\circ/10^\circ$, the tests resulted in a fracture of the fly-cutter after the exponential wear range was reached. The highest tool life with $L_T = 22.8 \text{ m}$ was achieved by the variant with a pressure angle $\alpha_{n,l/r} = 25^\circ/10^\circ$. The variants with the pressure angles $\alpha_{n,l/r} = 22.5^\circ/12.5^\circ$ and $\alpha_{n,l/r} = 22.5^\circ/12.5^\circ \text{ P}$ achieved a lower tool life compared to the variant $\alpha_{n,l/r} = 25^\circ/10^\circ$ with a tool life $L_T = 21.61 \text{ m}$ and $L_T = 19.07 \text{ m}$. A direct comparison of the three variants showed a difference in the rake face condition. The rake face of the variant $\alpha_{n,l/r} = 22.5^\circ/12.5^\circ$ was exposed to higher stresses. In addition to oxidation effects of smaller areas of the rake face (highlighted by a blue circle in Fig. 9),

adhesion of the material to the rake face was also observed (highlighted by a yellow circle in Fig. 9).

The results of the fly-cutting trials show that variants with a small pressure angle ($\alpha_{n,l} < 15^\circ$) on the leading flank have a shorter tool life than variants with a larger pressure angle. To further investigate this effect, the variants with the largest differences in the pressure angles were compared in Fig. 10.

The wear in area A on the trailing flank was almost identical for all variants. Differences between the variants can be identified at the leading flank in area A. High abrasive wear was observed for the variants $\alpha_{n,l/r} = 10^\circ/25^\circ$ and $\alpha_{n,l/r} = 12.5^\circ/22.5^\circ \text{ P}$. This wear formation is not recogniz-

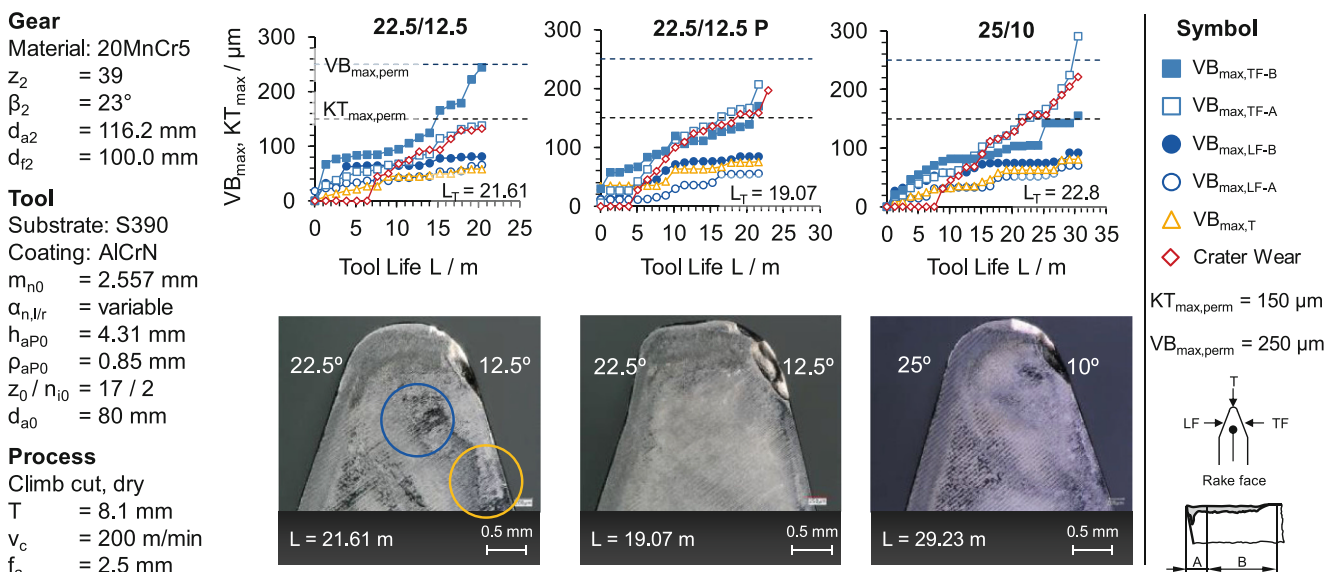


Fig. 9 Results of the fly-cutting trials for the variants 22.5/12.5, 22.5/12.5 P and 25/10

Gear
 Material: 20MnCr5
 $z_2 = 39$
 $\beta_2 = 23^\circ$
 $d_{a2} = 116.2 \text{ mm}$

Tool
 Substrate: S390
 Coating: AlCrN
 $m_{n0} = 2.557 \text{ mm}$
 $\alpha_{n,lr} = \text{variable}$
 $h_{aP0} = 4.31 \text{ mm}$
 $\rho_{aP0} = 0.85 \text{ mm}$
 $z_0 / n_{i0} = 17 / 2$
 $d_{a0} = 80 \text{ mm}$

Process
 Climb cut, dry
 $T = 8.1 \text{ mm}$
 $v_c = 200 \text{ m/min}$
 $f_a = 2.5 \text{ mm}$

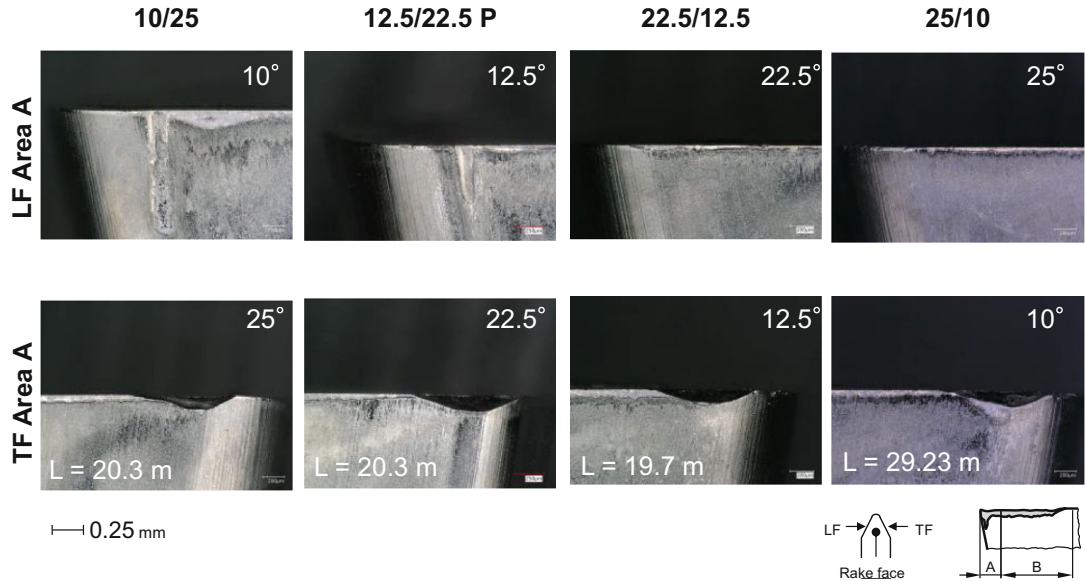


Fig. 10 Comparison of the leading and trailing flanks

able in the opposite variants. A possible cause for the development of the flank wear is a decrease of the effective clearance angles on the leading flank. The wear pattern of the trailing flanks of the variants $\alpha_{n,lr} = 25^\circ/10^\circ$ and $\alpha_{n,lr} = 22.5^\circ/12.5^\circ$ P corresponds to the wear that could also be identified in all other variants.

For a further analysis, the effective clearance angles φ_{eff} of the variants considered in Fig. 11 were calculated with SPARTapro. For the variant with the pressure angles $\alpha_{n,lr} = 10^\circ/25^\circ$, the effective clearance angles on the leading side are $\varphi_{\text{eff}} = 1.2^\circ$. This value increases to $\varphi_{\text{eff}} = 4.6^\circ$ for the trailing flank.

For the variant with a pressure angle $\alpha_{n,lr} = 12.5^\circ/22.5^\circ$ P, a higher value of $\varphi_{\text{eff}} = 1.6^\circ$ was initially obtained on the leading flank compared to the variant $\alpha_{n,lr} = 10^\circ/25^\circ$. The magnitude of the effective clearance angle is lower than for the $\alpha_{n,lr} = 10^\circ/25^\circ$ variant in the protuberance region (the light blue area in Fig. 11) due to the low protuberance profile angle of $\alpha_{\text{prP0}} = 9^\circ$. The influence of α_{prP0} on the course of the effective clearance angle can also be identified on the trailing flank. Analogous to the leading flank, a decrease in the effective clearance angle occurred in the protuberance region. However, with an effective clearance angle $\varphi_{\text{eff}} = 3^\circ$, this value is higher in the region of the protuberance than on the leading flank. For the variant with a pressure angle

Gear
 $z_2 = 39$
 $\beta_2 = 23^\circ$
 $d_{a2} = 116.2 \text{ mm}$

Tool
 $m_{n0} = 2.557 \text{ mm}$
 $\alpha_{n,lr} = \text{variable}$
 $\rho_{aP0} = 0.85 \text{ mm}$
 $z_0 / n_{i0} = 17 / 2$
 $d_{a0} = 80 \text{ mm}$

Process
 Climb cut, dry
 $T = 8.1 \text{ mm}$
 $v_c = 200 \text{ m/min}$
 $f_a = 2.5 \text{ mm}$

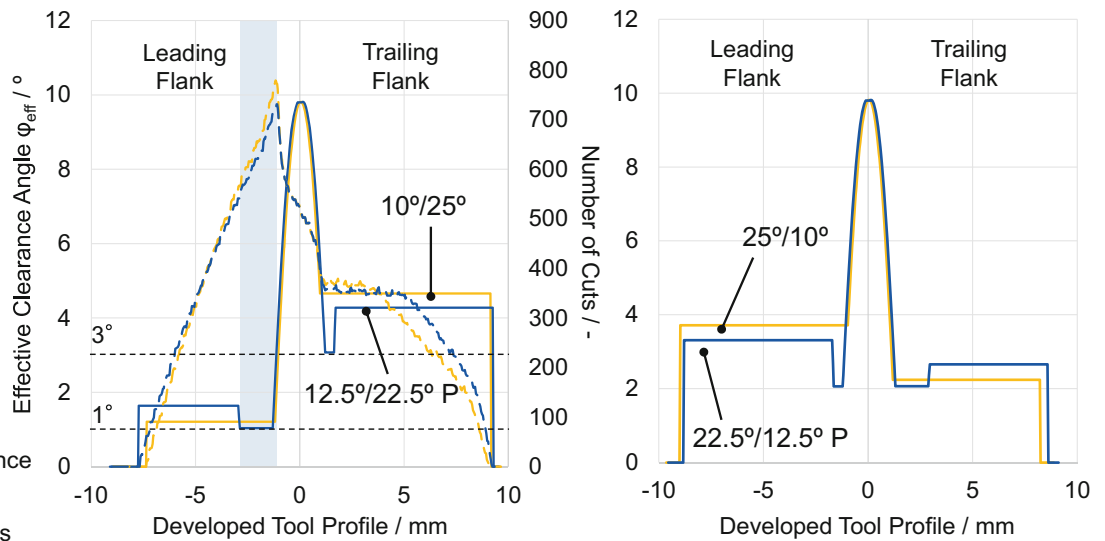


Fig. 11 Comparison of the effective clearance angle φ_{eff} for the critical variants

Gear
 Material: 20MnCr5
 $z_2 = 39$
 $\beta_2 = 23^\circ$
 $d_{a2} = 116.2 \text{ mm}$

Tool
 Substrate: S390
 Coating: AlCrN
 $m_{n0} = 2.557 \text{ mm}$
 $\alpha_{n,lr} = \text{variable}$
 $\rho_{aP0} = 0.85 \text{ mm}$
 $z_0 / n_{i0} = 17 / 2$
 $d_{a0} = 80 \text{ mm}$

Process
 Climb cut, dry
 $T = 8.1 \text{ mm}$
 $v_c = 200 \text{ m/min}$
 $f_a = 2.5 \text{ mm}$

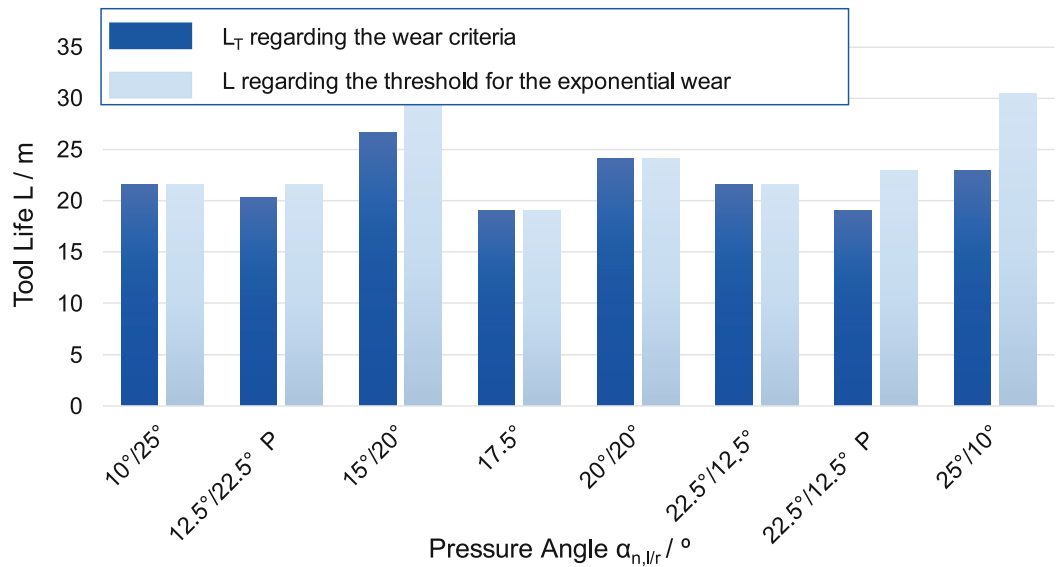


Fig. 12 Comparison of the tool life L_T for the different variants

$\alpha_{n,lr} = 22.5^\circ/12.5^\circ \text{ P}$, there was also a decrease in the course of the effective clearance angle in the area of the protuberance. With an effective clearance angle $\varphi_{\text{eff}} = 2^\circ$ in the area of the protuberance on the leading and trailing flank, low values resulted. However, no flank wear was found for this variant on the leading flank. Thus, an effective clearance angle of $\varphi_{\text{eff}} = 2^\circ$ seems to be a critical limit value for this tool/workpiece combination.

Finally, an investigation was carried out with regard to the locally occurring flank wear on the leading flank of the variant $\alpha_{n,lr} = 10^\circ/25^\circ$. Considering the effective clearance angle with $\varphi_{\text{eff}} = 1.2^\circ$, a continuous wear is to be expected. To explain this phenomenon, in the left diagram of Fig. 11 the course of the effective clearance angle φ_{eff} was superimposed with the number of cuts over the developed tool profile for the critical variants $\alpha_{n,lr} = 10^\circ/25^\circ$ and $\alpha_{n,lr} = 12.5^\circ/22.5^\circ \text{ P}$ since the other two variants were not subject to flank wear on the. The maximum number of cuts occurs in the area where the flank wear occurred on the tool flank. Furthermore, a superposition of the maximum number of cuts and the reduction of the effective clearance angle due to the protuberance can be identified for the variant $\alpha_{n,lr} = 12.5^\circ/22.5^\circ \text{ P}$. A combination of a small effective clearance angles with a high number of cuts favors the development of flank wear on the leading flank.

Figure 12 shows a comparison of all the variants investigated with regard to the tool life L_T and the tool life until the exponential wear range is reached. The diagram shows that the selected wear criteria correlate well with the onset of the exponential wear range.

The wear criteria for the maximum permissible wear mark width $VB_{\text{max,perm}} = 250 \mu\text{m}$ and for the maximum permissible crater depth of $KT_{\text{max,perm}} = 150 \mu\text{m}$ predominantly

represent the limit for the exponential wear range. Furthermore, the comparison of the variants shows the negative influence of small pressure angles on the tool life L_T . Further comparisons imply a likewise negative influence of the presence of protuberances on the respective tool life L_T . This negative influence can be attributed to a reduction of the clearance angle. This effect was observed among others by Kühn [18]. The variants $\alpha_{n,lr} = 22.5^\circ/12.5^\circ$ and $\alpha_{n,lr} = 12.5^\circ/22.5^\circ \text{ P}$ showed the lowest tool life L_T next to the reference variant.

5 Summary and outlook

Asymmetrical gears have advantages in applications with a preferred load direction, such as automotive transmissions or wind turbines. However, there are very few studies on the manufacturability of asymmetric gears. The objective of this report was to investigate the influence of asymmetrical profiles on the wear behavior of tools for the first time. Starting from a standard tool geometry used at the WZL of RWTH Aachen University for fly-cutting trials, seven further variants were defined for investigation. In addition to a second symmetrical variant, six variants were defined with different pressure angles on the leading and trailing flanks. Two of these variants also had a protuberance. To support the analysis, a simulative variant calculation including a graphical evaluation was implemented. An analysis of the maximum chip thickness $h_{\text{cu,max}}$ does not provide any meaningful information. With an increasing pressure angle $\alpha_{n,l}$ on the left side, the load shifts from the trailing to the leading flank. In the fly-cutting trials, in addition to the attainment of predefined wear criteria, the attainment

of the exponential wear rate was also investigated. The results showed that variants with a small pressure angle on the leading flank develop flank wear. This wear formation is not recognizable in the opposite variants with a large pressure angle. The tool life L_T of the variants with a small pressure angle on the leading flank was lower than the tool life of other variants. In addition, a protuberance also implies a low tool life L_T . A simulative analysis showed that variants with a small pressure angle on the leading flank also have a small effective clearance angle φ_{eff} . In combination with a superimposition of a maxima of number of cuts, a small effective clearance favors flank wear. In the future, the observed phenomena need to be further investigated. In particular, the influence of the clearance angle and the protuberance on the tool life of asymmetric variants needs to be analyzed in further studies.

Funding The authors gratefully acknowledge the Federal Ministry for Economic Affairs and Energy for providing the financial support for the project IGF 20315N based on a resolution of the German Parliament. The research was also supported by the Gear Research Circle of the WZL of RWTH Aachen University.

Funding Open Access funding enabled and organized by Projekt DEAL.

Conflict of interest C. Janßen, J. Brimmers and T. Bergs declare that they have no competing interests.

Open Access This article is licensed under a Creative Commons Attribution 4.0 International License, which permits use, sharing, adaptation, distribution and reproduction in any medium or format, as long as you give appropriate credit to the original author(s) and the source, provide a link to the Creative Commons licence, and indicate if changes were made. The images or other third party material in this article are included in the article's Creative Commons licence, unless indicated otherwise in a credit line to the material. If material is not included in the article's Creative Commons licence and your intended use is not permitted by statutory regulation or exceeds the permitted use, you will need to obtain permission directly from the copyright holder. To view a copy of this licence, visit <http://creativecommons.org/licenses/by/4.0/>.

References

- Deng G, Nakanishi T (2001) Enhancement of bending load carrying capacity of gears using an asymmetric involute tooth. *MPT II.01.202*, pp 513–517 <https://doi.org/10.1299/jsmeimpt.II.01.202.513>
- Stahl K, Höhn B-R, Otto M, Fröh A (2012) Normberechnung der Geometrie und Tragfähigkeit von asymmetrischen Evolventenverzahnungen. *Z Wirtsch Fabrikbetr* 2012:293
- Ingeli J, Brumm M (2015) Asymmetrische Zahnstückengeometrie: Untersuchung des Einflusses von asymmetrischen Zahnstückengeometrien auf das Laufverhalten von Stirnrad-Verzahnungen. Abschlussbericht; Forschungsvorhaben Nr. 484 I. FVA, Frankfurt
- Niemann G, Winter H (2004) *Maschinenelemente: Band 3: Schraubrad-, Kegelrad-, Schnecken-, Ketten-, Riemen-, Reibradgetriebe, Kupplungen, Bremsen, Freiläufe*, 2nd edn. vol 3. Springer, Berlin
- Plewnia C (1992) *Drehübertragungs- und Geräuschverhalten bogenverzahnter Kegelradgetriebe*. RWTH Aachen University, Aachen (Diss)
- Schweicher WM (1994) *Rechnerische Analyse und Optimierung des Beanspruchungsverhaltens bogenverzahnter Kegelräder*. RWTH Aachen University, Aachen (Diss)
- Bergs T (2018) Cutting force model for gear honing. *CIRP Ann Manuf Technol* 67:53–56. <https://doi.org/10.1016/j.cirp.2018.03.022>
- Herzhoff P (2003) *Trockenbearbeitung und Minimalmengenschmierung beim Wälzfräsen mit HSS-Werkzeugen*. Otto-von-Guericke-Universität, Magdeburg (Diss)
- Winkel O (2005) *Steigerung der Leistungsfähigkeit von Hartmetallwälzfräsern durch eine optimierte Werkzeuggestaltung*. RWTH Aachen University, Aachen (Diss)
- Schalaster R (2012) *Optimierung des Fertigwälzfräsens von Verzahnungen*. RWTH Aachen University, Aachen (Diss)
- Stuckenberg A (2014) *Vermeidung von Oberflächendefekten beim Wälzfräsen*. RWTH Aachen University, Aachen (Diss)
- Liu W, Ren D, Usui S, Wadell J, Marusich TD (2013) A gear cutting predictive model using the finite element method. *Procedia CIRP* 8:51–56. <https://doi.org/10.1016/j.procir.2013.06.064>
- Rech J (2006) Influence of cutting edge preparation on the wear resistance in high speed dry gear hobbing. *Wear* 261:505–512. <https://doi.org/10.1016/j.wear.2005.12.007>
- Bouzakis K-D, Lili E, Michailidis N, Friderikos O (2008) Manufacturing of cylindrical gears by generating cutting processes: a critical synthesis of analysis methods. *CIRP Ann Manuf Technol* 57:676–696
- Köchig M (2019) *Analyse geometrischer Einflüsse auf die Werkzeugbelastung beim Wälzfräsen*. Otto-von-Guericke-Universität, Magdeburg
- Klocke F, Brecher C (2017) *Zahnrad- und Getriebetechnik: Auslegung – Herstellung – Untersuchung – Simulation*, 1st edn. Hanser, München
- NormNorm Einsatzstähle. Technische Lieferbedingungen(10084)
- Kühn F (2020) *Auslegung der Makro- und Mikrogeometrie von Wälzfräserschneiden: Design of the macro and micro geometry of hob cutting edges*, 1st edn. Ergebnisse aus der Produktionstechnik Technologie der Fertigungsverfahren, 2020. vol 32. Apprimus, Aachen
- Mattox DM (2010) *Handbook of physical vapor deposition (PVD) processing*, 2nd edn. William Andrew, Oxford
- Brecher C, Brumm M, Krömer M (2015) Design of gear hobbing processes using simulations and empirical data. *Procedia CIRP* 33:484–489. <https://doi.org/10.1016/j.procir.2015.06.059>
- Weck M, Winter W, Klocke F, Winkel O (2003) Analysis of gear hobbing processes by manufacturing simulation. *Ann Ger Acad Soc Prod Eng* 10:55–58
- Klocke F, König W (2008) *Fertigungsverfahren 1: Drehen, Fräsen, Bohren*, 8th edn. VDI-Buch. Springer, Berlin
- Troß N, Brimmers J, Bergs T (2021) Tool wear in dry gear hobbing of 20MnCr5 case-hardening steel, 42CrMo4 tempered steel and EN-GJS-700-2 cast iron. *Wear*. <https://doi.org/10.1016/j.wear.2021.203737>